

A nanosecond level current pulse capture taper optical fiber probe based on micron level nitrogen-vacancy color center diamond

Yuchen Bian(卞雨辰), Yangfan Mao(毛扬帆), Honghao Chen(陈鸿浩), Shiyu Ge(葛仕宇), Wentao Lu(卢文韬), Chengkun Wang(王成坤), Sihan An(安思瀚), and Guanxiang Du(杜关祥)

Citation: Chin. Phys. B, 2024, 33 (**12**): 120301. DOI: 10.1088/1674-1056/ad78da
Journal homepage: http://cpb.iphy.ac.cn; http://iopscience.iop.org/cpb

What follows is a list of articles you may be interested in

Verifying hierarchical network nonlocality in general quantum networks

Shu-Yuan Yang(杨舒媛), Jin-Chuan Hou(侯晋川), and Kan He(贺衍)
Chin. Phys. B, 2024, 33 (**7**): 070304. DOI: 10.1088/1674-1056/ad3dd5

Exceptional points and quantum dynamics in a non-Hermitian two-qubit system

Yi-Xi Zhang(张益玺), Zhen-Tao Zhang(张振涛), Zhen-Shan Yang(杨震山), Xiao-Zhi Wei(魏晓志), and Bao-Long Liang(梁宝龙)
Chin. Phys. B, 2024, 33 (**6**): 060308. DOI: 10.1088/1674-1056/ad2a70

Wigner function of optical cumulant operator and its dissipation in thermo-entangled state representation

Ke Zhang(张科), Lan-Lan Li(李兰兰), and Hong-Yi Fan(范洪义)
Chin. Phys. B, 2024, 33 (**6**): 060307. DOI: 10.1088/1674-1056/ad2f20

Quantum correlations and entanglement in coupled optomechanical resonators with photon hopping via Gaussian interferometric power analysis

Y. Lahlou, B. Maroufi, and M. Daoud
Chin. Phys. B, 2024, 33 (**5**): 050303. DOI: 10.1088/1674-1056/ad2a6e

Quantum correlations and entanglement in coupled optomechanical resonators with photon hopping via Gaussian interferometric power analysis

Y. Lahlou, B. Maroufi, and M. Daoud
Chin. Phys. B, 2024, 33 (**5**): 050303. DOI: 10.1088/1674-1056/ad2a6e

---

SPECIAL TOPIC — Quantum computing and quantum sensing

A nanosecond level current pulse capture taper optical fiber probe based on micron level nitrogen-vacancy color center diamond

Yuchen Bian(卞雨辰)[1], Yangfan Mao(毛扬帆)[2], Honghao Chen(陈鸿浩)[2], Shiyu Ge(葛仕宇)[2], Wentao Lu(卢文韬)[1], Chengkun Wang(王成坤)[2], Sihan An(安思瀚)[2], and Guanxiang Du(杜关祥)[1,†]

[1] *Portland Institute, Nanjing University of Posts and Telecommunications, Nanjing* 210000, *China*

[2] *College of Telecommunication and Information Engineering, Nanjing University of Posts and Telecommunications, Nanjing* 210000, *China*

(Received 27 July 2024; revised manuscript received 28 August 2024; accepted manuscript online 10 September 2024)

This work demonstrates a micron-sized nanosecond current pulse probe using a quantum diamond magnetometer. A micron-sized diamond crystal affixed to a fiber tip is integrated on the end of a conical waveguide. We demonstrate real-time visualization of a single 100 nanosecond pulse and discrimination of two pulse trains of different frequencies with a coplanar waveguide and a home-made PCB circuit. This technique finds promising applications in the display of electronic stream and can be used as a pulse discriminator to simultaneously receive and demodulate multiple pulse frequencies. This method of detecting pulse current is expected to provide further detailed analysis of the internal working state of the chip.

Keywords: pulse capture, nitrogen-vacancy (NV) color center, current imaging, chip detection

PACS: 03.65.–w, 03.65.Aa, 03.67.–a, 02.20.Uw **DOI:** 10.1088/1674-1056/ad78da

1. Introduction

In previous studies, the nitrogen-vacancy (NV) center has often been used as highly sensitive magnetic field sensors to image the magnetic field generated by the current distribution of integrated circuits. Currently, two commonly used NV center detection systems exist. The first is the single NV center system, which collects weak fluorescence over a significant accumulation of detection time using a single-photon system to complete measurements. Despite this, it achieves a sensitivity level of nT/$\sqrt{\text{Hz}}$.[1–3] The second method involves wide-field imaging, utilizing a large-area diamond thin film and a CCD camera to image the static magnetic field over a broad chip region. This approach allows for rapid quasi-static analysis of large-area current distributions and can achieve different spatial resolution imaging based on the concentration of NV centers.[4,5]

However, integrated circuits often contain numerous dynamic periodic pulsed currents constrained by internal clock frequencies.[6] The distribution of these currents, with varying frequencies and timing sequences, often contains critical information about the chip's operational state at a given time.[7] The traditional methods mentioned above have limitations. The single NV center system requires extensive detection time, making it unsuitable for probing chips with constantly changing operational states.[8] On the other hand, the wide-field imaging approach treats pulsed currents as quasi-static, providing only a rough overview of the working area's distribution. It cannot capture temporal and intensity data of the currents or provide a more detailed analysis of the working area's distribution.[9]

In this paper, we have fabricated a tapered fiber probe with a spatial resolution of 2 μm by attaching a 2 μm diamond block to the end of a tapered fiber, enabling it to detect chip-level transmission lines. Then we used a coplanar waveguide with a transmission line width of 100 μm as the test subject. Through a tapered optical fiber diamond probe at the micrometer level, we achieved nanosecond-level pulse capture on the surface transmission line using CW laser detection.[10] In the time-domain analysis, we employed an oscilloscope with a noise reduction algorithm[11] to capture individual hundred-nanosecond-level current pulses in real-time. For the frequency-domain analysis, we utilized a spectrum analyzer with a rapid frequency sweep analysis method to capture periodic pulse trains with a minimum duration of ten nanoseconds. Finally, we employed this technology to locate and image two transmission lines carrying pulsed currents of different frequencies on a self-made PCB board. We hope to demonstrate the application prospects of this study in capturing individual current pulses inside the chip and locating the areas where current pulses of different frequencies are generated.

2. Basic theory and experimental setup

The Hamiltonian of the NV color center is expressed as

$$H = D \cdot S_Z^2 + E \cdot \left(S_X^2 - S_Y^2\right) - \gamma_e \cdot \boldsymbol{B} \cdot \boldsymbol{S}. \tag{1}$$

We sense the pulsed magnetic field through the Hamiltonian term $\gamma_e \cdot \boldsymbol{B} \cdot \boldsymbol{S}$, and the electron spin magnetic ratio γ_e is

†Corresponding author. E-mail: duguanxiang@njupt.edu.cn

© 2024 Chinese Physical Society and IOP Publishing Ltd

2.8 MHz/Gauss. Our system comprises an APD, spectrum analyzer, oscilloscope, microwave source, as well as a tapered optical fiber probe and a tapered antenna. It eliminates the need for complex pulse control and utilizes the combination of a fiber-optic NV center and a tapered antenna to sense pulsed currents in close proximity to the waveguide under test. The NV center probe is made of a 2.025 μm NV center block, so it has a spatial resolution of 2 μm. Additionally, due to the highest fluorescence intensity of zero-field ODMR, the system does not require the use of magnets to split the energy levels of the color center.

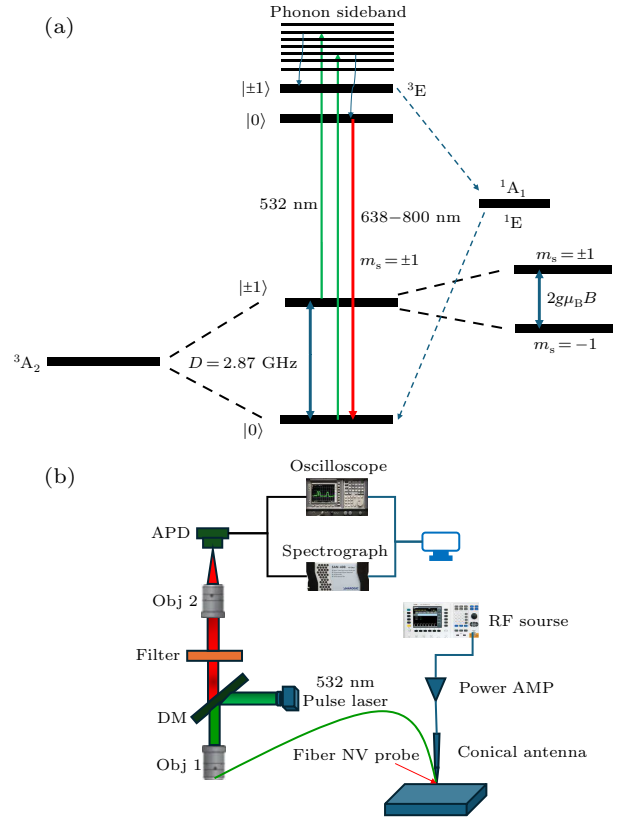


Fig. 1. (a) The energy level structure of color center. We use the Zeeman effect to sense pulsed magnetic fields. (b) Experimental system structure diagram.

Initially, the physical implementation of our combined probe is illustrated in Fig. 2(a). We have designed the coplanar waveguide with a tapered shape and affixed a loop of gold wire at its distal end to generate a strong microwave magnetic field. This allows our optical fiber probe to traverse through the coil. Under the condition of acquiring a sufficiently intense microwave excitation, it can approach the test object as closely as possible, enabling it to detect pulse currents that are sufficiently weak and of sufficiently short duration.

Both the microwave source and the laser operate in CW mode, and the pulse current to be measured is generated by passing a current from a current source through a chip transmission line controlled by a TTL switch. As depicted in Fig. 2(c), the ODMR curve adheres to the Lorentzian fitting formula

$$I(\omega;A,P,w,f_0) = P + \frac{\mathrm{A}w}{(\omega-\omega_0)^2+w^2}. \tag{2}$$

The pulse current with a specific frequency generated by the pulse generator induces a corresponding spectral line shift of the zero-field ODMR at the same frequency due to its magnetic field. Consequently, the resulting fluorescence response exhibits periodic amplitude variations, enabling us to acquire and analyze the fluorescence signal to determine the operational frequency of the pulse current and its location of action, among other disturbing currents.[12]

In our experiments, the capture of pulse currents is achieved through the continuous splitting and rebound of the energy levels of color center electrons as currents are generated and dissipated (Zeeman effect).[13,14] As shown in Fig. 2(c), the energy level split resulting from the magnetic field of pulse currents causes the ODMR spectral line broadening, if we lock MW frequency at 2877 MHz, due to the broadening of spectral lines, fluorescence intensity differences will occur as ΔC. And this response in quantum physics is almost instantaneous, making it highly sensitive to instantaneous magnetic fields. Similar to using NV center as a frequency-modulated RF signal receiver,[15] they can also serve as a receiver for pulse currents of different frequencies. By using an oscilloscope and spectrum analyzer, we can read out the frequency and intensity changes of the fluorescence signal, thus capturing the pulse current. To achieve a signal with a high signal-to-noise ratio, we utilize the zero-field ODMR for pulse capture, as it offers a fluorescence intensity four times greater than that of single-peak ODMR. We fix the microwave frequency at the waist of the ODMR peak, ensuring optimal pulse detection sensitivity. As illustrated in Fig. 2(d), laser readout occurs during the period of color center energy level changes. To sense pulse currents with the shortest possible pulse width, we need to ensure that the laser fully polarizes the electron spins of the NV centers within the brief duration of energy level alteration,[16] thereby capturing the timing of the energy level changes. Therefore, throughout the experiment, we maintain the laser intensity at its maximum to optimize the system's ability to read out the energy level changes.[17,18]

In the subsequent experiments, we define the fluorescence contrast as the ratio of the fluorescence intensity difference at the time of energy level change to the baseline fluorescence

$$\Delta C = \frac{I - I_0}{I}. \tag{3}$$

The fluorescence contrast acquired by our detection system arises from the spin polarization of the electronic energy levels by the laser during the period of energy level transitions. According to the optical polarization spin rate equation[19]

$$\frac{\mathrm{d}\rho}{\mathrm{d}t} = \frac{1}{\mathrm{i}\hbar}[H,\rho] + \left\{\frac{\mathrm{d}\rho}{\mathrm{d}t}\right\}_{\mathrm{incoh}}, \tag{4}$$

if the pulse width and period of the pulsed current gradually decrease, the laser's read-out time for the energy levels will correspondingly shorten, leading to increasingly incomplete polarization of the color centers and a subsequent decrease in contrast. This phenomenon imposes limitations on the detectable pulse width and frequency range of our system. In the subsequent experiments, we will conduct in-depth discussions and verifications on this issue, and present the measurable pulse width, detection frequency range, detection sensitivity, and other performance indicators of the system for pulsed currents. Next, we will use a NV center probe to capture the current pulse in both time and frequency domains. Time domain capture is mainly used to observe the waveform of a single pulse in real time, while frequency domain capture is mainly used to locate the generation location of specific frequency current pulses.

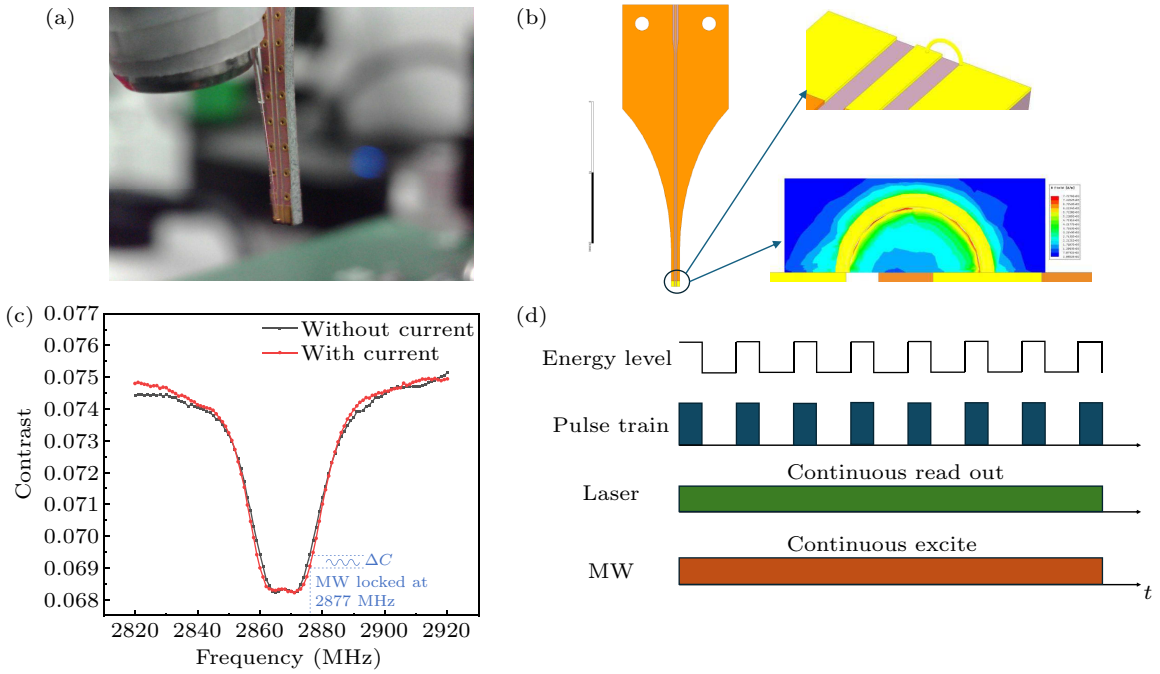


Fig. 2. (a) The combination detection diagram of the actual optical fiber probe and the conical waveguide. (b) Simulation diagram of microwave field for gold wire at the end of a tapered waveguide. (c) The comparison of CW ODMR with and without current. (d) Both the laser and microwave are operated in CW mode, allowing for continuous reading and excitation of the color centers.

3. Time-domain pulse catch

First, we conducted a verification experiment to validate the system's capability of capturing current pulse waveforms in the time domain. Using a pulse generator, we generated a single pulse with a pulse width of 100 ns on the coplanar waveguide. Subsequently, we captured the fluorescence signal returned by the color centers using an oscilloscope with a sampling rate of 10 Gs. After using Gaussian filtering noise reduction algorithm, we obtained a fluorescence response that closely matched the reference pulse (Fig. 3).

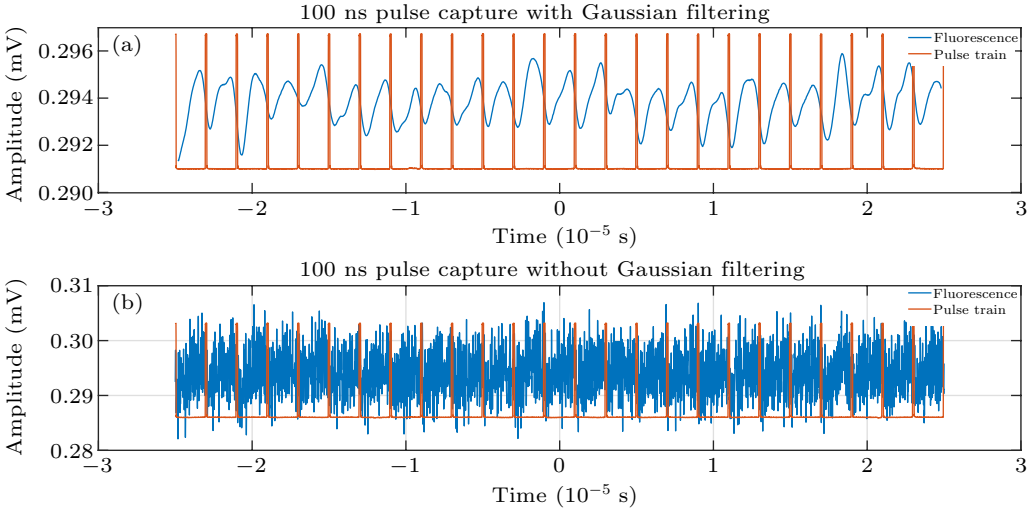


Fig. 3. The captured data of the 100 ns current pulse demonstrates the alignment between the denoised fluorescence signal and the reference pulse.

In the previous experiments, we demonstrated the real-time capture of pulse current waveforms. However, in chip applications, pulse currents are often in the form of pulse trains with fixed periodic frequencies, and there is a need for scanning and imaging of the working area. Therefore, for periodic signals, we adopted a frequency domain analysis approach to extract the intensity and frequency information of the periodic pulse currents and applied it to imaging of the working area. Based on this principle, we used a 100 μm wide transmission line on a coplanar waveguide as a carrier for passing pulse currents, and performed spectral analysis and surface magnetic field imaging of the pulse currents.

4. Frequency-domain detection sensitivity

Subsequently, we estimated the minimum detectable magnetic field and sensitivity of the induced pulse magnetic field within the spectral system. Initially, we performed a Lorentzian fit on the zero-field ODMR spectrum depicted in Fig. 2(c) to obtain its mathematical expression

$$I = 0.075 - \frac{0.6}{\pi} \times \frac{25}{4(\omega - 2867)^2 + 625}. \tag{5}$$

With the microwave frequency fixed at 2877 MHz (the maximum slope point of the expression), we define the fluorescence intensities with and without the presence of the pulsed magnetic field as I_0 and I, respectively. The RBW parameter of the spectrum analyzer employed in our experiments is set to 3 Hz. After measurement of our system this RBW value in our system indicates that the instrument can minimally resolve periodic signals with a power spectral density that is 20 ppm higher than the basal signal. Given the information provided, we can deduce that the minimum resolvable fluorescence contrast can be estimated using the following equation:

$$\frac{I - I_0}{I} = 20 \text{ ppm}. \tag{6}$$

By substituting the fluorescence intensities I_0 and I into Eq. (5), we can solve for the two horizontal coordinates ω_0 and ω that correspond to a fluorescence difference of 20 ppm. Based on the magnetic gyromagnetic ratio of the NV color center, the minimum detectable pulse magnetic field strength of this system can be determined as follows:

$$B_{\min} = \frac{\omega_0 - \omega}{\gamma_e}. \tag{7}$$

Based on the preceding discussion, the sensitivity formula for measuring pulse magnetic fields using this system can be expressed as follows:

$$\delta = B_{\min}/\sqrt{\text{RBW}}. \tag{8}$$

At this point, we substitute the known $\omega = 2877$ MHz into Eq. (5), and based on Eqs. (6)–(8), we can get $B_{\min} = 138$ nT, $\delta = 79.7\ \text{nT}/\sqrt{\text{Hz}}$.

5. Frequency-domain pulse discriminator

In the subsequent experiments, we injected pulse trains with a fixed frequency of 500 kHz into the transmission line and gradually altered their duty cycle to examine the pulse width range capable of capturing pulse trains. A significant dependency between spectral intensity and pulse width was observed. As the pulse width decreased to the order of 10 ns, the fluorescence contrast ratio decreased significantly due to the drastic reduction in the time reserved for laser polarization. Consequently, it became challenging to observe the waveform in the time domain. However, in the frequency domain, as shown in Fig. 4(a), we effectively acquired fluorescence data with a polarization time of 10 ns by continuously reducing the RBW parameter of spectral analysis to 3 Hz, which minimized the background noise. The results indicated that we successfully captured periodic pulses with a minimum pulse width of 10 ns through spectral analysis.

Furthermore, as the frequency of the pulsed current increases, both the high and low-level time thresholds of the pulsed current decrease simultaneously, leading to a decrease in the laser's reading time for these two energy level transitions. Consequently, the intensity of the spectral signal also decreases, affecting the minimum detectable pulse period. Therefore, we subsequently fixed the duty cycle of the current pulse at 50% and gradually varied its frequency to determine the frequency range of the pulsed current detectable by our system. As shown in Fig. 4(b), based on an RBW parameter of 3 Hz, we were able to detect pulse signals with a minimum frequency of 20 MHz.

We further investigated the system's performance by scanning and imaging the waveguide using spectral intensity. We compared the obtained scan image with a simulation image, which shows a good agreement. This confirms the capability of spectral analysis for imaging pulse currents.

Finally, we devised a sophisticated experiment to verify the capability of our pulse capture method in locating the position of a specific frequency pulsed current while shielding interference from surrounding magnetic fields. To mimic the environment within a chip where multiple signals of different frequencies are transmitted concurrently over various transmission lines, we designed a PCB board featuring two transmission lines with a line width of 100 μm and a separation distance of 100 μm. These transmission lines were capable of carrying pulsed currents of varying frequencies generated by a pulse generator. Firstly, to verify the ability of the color center to simultaneously receive multiple frequency current pulses, we simultaneously applied pulse currents with frequencies of 500 kHz and 505 kHz to two transmission lines, and successfully observed the current spectra of both on the spectrometer (Fig. 5(a)). Next, we conducted frequency localization

experiments on these two transmission lines using a scanning imaging system. Through the LabVIEW program, we simultaneously controlled the spectrometer, displacement stage and pulse generator. After setting the laser and microwave to CW mode and passing the fiber optic probe through the conical waveguide near the transmission line to be tested, we connected the APD output to the spectrometer. During the imaging process, every time the displacement table moved, we used instructions to simultaneously obtain spectral data of two pulse frequency points from the spectrometer, and used their respective spectral intensity values to draw imaging maps. We positioned fiber optic probe between the two transmission lines and simultaneously applied 500 kHz and 1 MHz pulsed currents to the respective lines. By utilizing the NV center as a frequency discriminator, we measured the spectral intensity at two distinct frequency points and conducted a simultaneous scanning imaging of both transmission lines. As shown in the results of Fig. 5(c), the two scanning images accurately reflect the relative positions of the two transmission lines and effectively shield the magnetic field interference from neighboring non-detected frequency bands, thereby achieving accurate localization of the specific frequency pulsed current.

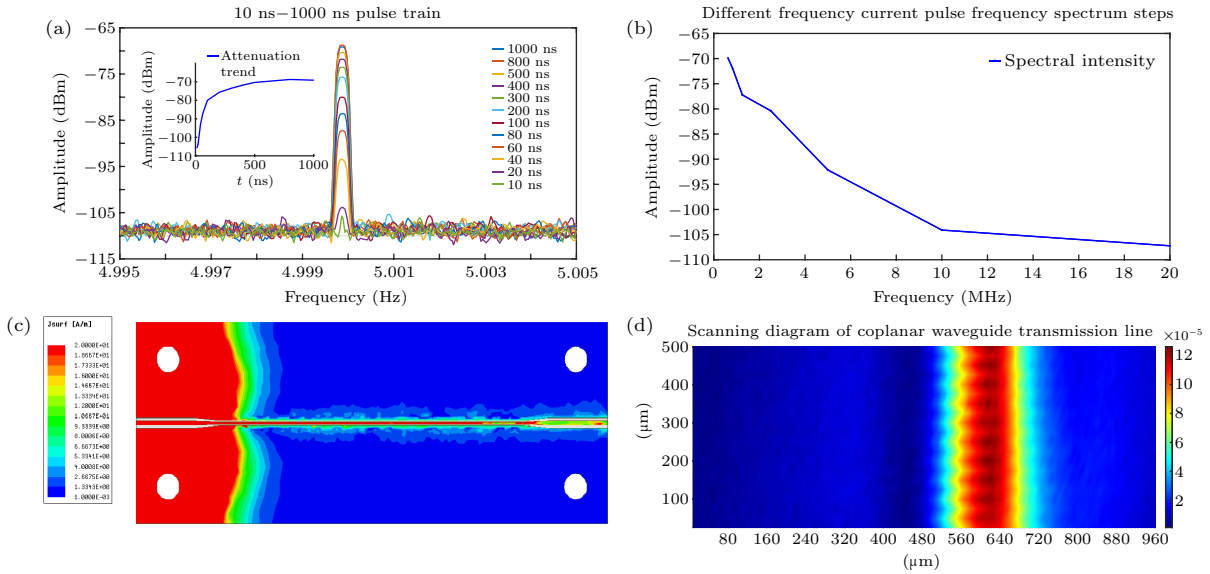


Fig. 4. (a) Fluorescence response spectrum of current pulses with different pulse widths at a fixed frequency of 500 kHz. (b) The fluorescence response spectrum staircase diagram of current pulses with different periods but a fixed duty cycle of 50%. (c) Simulation diagram of surface magnetic field after applying a 500 kHz pulse current to a coplanar waveguide. (d) Imaging diagram of a segment of coplanar waveguide transmission line using spectral signals.

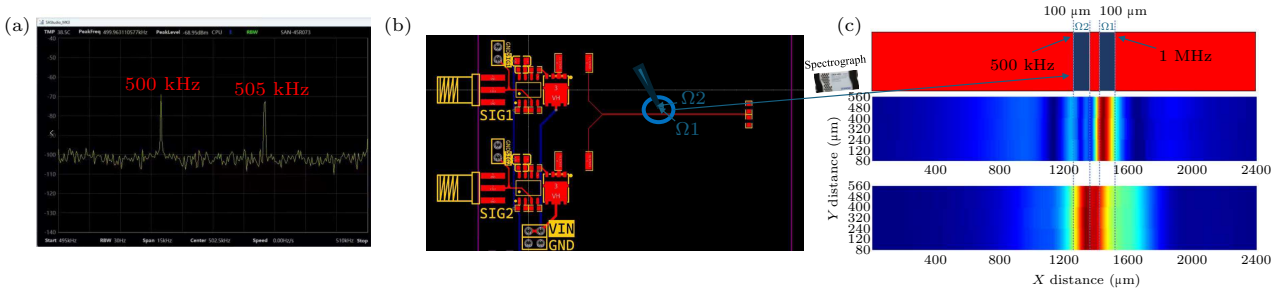


Fig. 5. (a) Spectrum diagram of color center receiving two types of pulse currents with frequencies of 500 kHz and 505 kHz simultaneously. (b) The PCB schematic diagram for a dual transmission line setup. (c) Two signals of 500 kHz and 1 MHz are simultaneously applied to two transmission lines on a PCB, and the two demodulated signals from the color centers are imaged concurrently, the resulting figure represents the operational locations or regions of the two frequency signals.

6. Conclusion and perspectives

In summary, we have realized a pulsed current detector utilizing NV color centers as a receiver of current frequencies whose spatial resolution can reach 2 μm. This device enables us to observe the waveform of individual 100 ns pulsed currents in the time domain, and also to capture extremely short periodic current pulses in the frequency domain. Detecting the spectrum of current pulses is an excellent method for scanning and imaging the working position of pulsed currents. We have estimated the minimum detectable magnetic field and detection sensitivity of color centers as current frequency discriminators, which are 138 nT and 79.7 nT/$\sqrt{\text{Hz}}$, respectively. Then we experimentally perceived periodic pulse trains with a minimum pulse width of 10 ns and a maximum frequency of 20 MHz. By utilizing the spectral intensity as the scanning value, we have conducted pulsed current scan-

ning imaging of coplanar waveguide transmission lines, which highly aligns with the simulation results. Finally, we tested the performance of the color center as a frequency discriminator for current frequencies using a self-made PCB board. The results demonstrate the detector's excellent capability in locating the position of pulsed currents with specific frequencies. Looking forward, through continuous optimization of the magnetic sensitivity of the color centers and the development of more advanced signal processing techniques, this technology is expected to be applied in detecting pulsed currents on actual chips and achieving precise positioning and imaging of their distributions based on frequency spectra. Based on this, effective analysis may be conducted on the real-time stream inside the chip and side channel of the chip.[20–22]

Acknowledgments

Project supported by the National Key R&D Program of China (Grant No. 2021YFB2012600). We extend our special thanks to the staff of Jiangsu Institute of Metrology for their guidance and selfless assistance.

References

[1] Dolde F, Fedder H, Doherty M W, Nobauer T, Rempp F, Balasubramanian G, Wolf T, Reinhard F, Hollenberg L C and Jelezko F 2011 *Nat. Phys.* **7** 459

[2] Glenn D R, Bucher D B, Lee J, Lukin M D, Park H and Walsworth R L 2018 *Nature* **555** 351

[3] Kehayias P, Levine E V, Basso L, Henshaw J, Ziabari M S, Titze M, Haltli R, Okoro J, Tibbetts D R, Udoni D M, Bielejec E, Lilly M P, Lu T M, Schwindt P D D and Mounce A M 2022 *Phys. Rev. Applied* **17** 014021

[4] Sengottuvel S, Mrozek M, Sawczak M, Głowacki J M, Ficek M, Gawlik W and Wojciechowsk A M 2022 *Scientific Reports* **12** 17997

[5] Nowodzinski A, Chipaux M, Toraille L, Jacques V, Roch J F and Debuisschert T 2015 *Microelectronics Reliability* **55** 1549

[6] Su Y C and Huang S Y 2022 *IEEE Transactions on Computer-Aided Design of Integrated Circuits and Systems* **42** 2761

[7] Heinrich H K 1990 *IBM Journal of Research and Development* **34** 162

[8] Ju Z P, He M T, Lin J J, Zhu J, Wu B T and Wu E 2022 *Results in Physics* **40** 105874

[9] Turner M J, Langellier N, Bainbridge R, Walters D, Meesala S, Babinec T M, Kehayias P, Yacoby A, Hu E, Lončar M, Walsworth R L and Levine E V 2020 *Phys. Rev. Applied* **14** 014097

[10] Gruber A, Draäbenstedt A, Tietz C, Fleury L, Wrachtrup J and Borczyskowski C V 1997 *Science* **276** 2012

[11] Ito K and Xiong K 2000 *IEEE Transactions on Automatic Control* **45** 910

[12] Saijo S, Matsuzaki Y, Saito S, Yamaguchi T, Hanano I, Watanabe H, Mizuochi N and Ishi-Hayase J 2018 *Appl. Phys. Lett.* **113** 082405

[13] Balasubramanian G, Chan I. Y, Kolesov R, Al-Hmoud M, Tisler J, Shin C, Kim C, Wojcik A, R P Hemmer, Krueger A, Hanke T, Leitenstorfer A, Bratschitsch R, Jelezko F and Wrachtrup J 2008 *Nature* **455** 648

[14] Shi Z Y, Gao W, Wang Q, Guo H, Tang J, Li Z H, Wen H F, Ma Z M and Liu J 2023 *Chin. Phys. B* **32** 070704

[15] Shao L B, Zhang M, Markham M, Edmonds A M and Lončar M 2016 *Phys. Rev. Applied* **6** 064008

[16] Bai R X, Yang F, Liu P, Gao T, Zhou L, Yin X H, Zhu X Y, Ma W H, He F Y, Chen N C, Sun Y, Ma J T, Yu T and Du G X 2022 *Appl. Phys. Lett.* **120** 044003

[17] Robledo L, Bernien H, Sar T V D and Hanson R 2011 *New J. Phys.* **13** 025013

[18] Gupta A, Hacquebard L and Childress L 2016 *J. Opt. Soc. Am. B* **33** B28

[19] Magaletti S, Mayer L, Roch J and Debuisschert T 2024 *New J. Phys.* **26** 023020

[20] Barry J F, Schloss J M, Bauch E, Turner M J, Hart C A, Pham L M and Walsworth R L 2020 *Rev. Mod. Phys.* **92** 015004

[21] Lin S Z, Wang Q, Guo H, Wen H F, Li Z H, Tang J, Ma Z and Liu J 2021 *Laser Phys. Lett.* **18** 115201

[22] Liu Y K, Liu Z H, Li Y, Ma Z M, Li Z H, Wen H F, Guo H, Tang J, Li Y J and Liu J 2024 *IEEE Transactions on Instrumentation and Measurement* **73** 1